Rolling-Horizon Electric Vertical Takeoff and Landing Arrival Scheduling for On-Demand Urban Air Mobility

Imke C. Kleinbekman* and Mihaela Mitici†
Delft University of Technology, 2926 HS Delft, The Netherlands
and
Peng Wei‡
Iowa State University, Ames, Iowa 50011

https://doi.org/10.2514/1.I010776

Urban air mobility with electric vertical takeoff and landing (eVTOL) vehicles is envisioned to become a fast and flexible urban transportation mode. Apart from technical challenges for eVTOLs regarding vehicle design and manufacturing, airspace design and traffic control mechanisms are most desired on the operation side. In particular, from an operational point of view, the arrival phase is expected to be the main bottleneck, with restricted vertiport resources, high air traffic density, frequent flight maneuvers, and limited eVTOL remaining battery energy, all leading to complex operational constraints. This work provides a framework to enable optimal and efficient on-demand eVTOLs arrivals in the context of on-demand urban air mobility. This paper investigates the throughput of a double-landing-pad vertiport by proposing a new vertiport terminal area airspace design and a novel rolling-horizon scheduling algorithm with route selection capability to compute the optimal required time of arrival for eVTOLs in a tactical manner. Finally, a case study on arrivals in a hexagonal vertiport network is performed to show the algorithm performance with different configurations. Our simulation results show that up to 50 s delay per eVTOL is expected during the commuter peak hours and less than 10 s delay is expected during off-peak hours.

I. Introduction

URBAN air mobility (UAM) with electric vertical takeoff and landing (eVTOL) vehicles is envisioned to become a customized, on-demand air transportation mode, by carrying passengers and cargo safely and efficiently within urban areas. As cities and streets become more congested, UAM offers the potential for significant commute time savings compared with ground transportation modes.

Companies such as Airbus, Bell, Embraer, Joby Aviation, Kitty Hawk, Pipistrel, Volocopter, and Aurora Flight Sciences have been designing, building, and testing innovative eVTOL aircraft for UAM operations [1]. The UAM industry is facing several challenges regarding vehicle design and manufacturing, such as battery technology, assured vehicle autonomy, and scalable manufacturing process. Moreover, in order to make UAM a reliable and practical transportation mode, operational challenges must be addressed. In particular, there is a need for airspace design and air traffic control mechanisms to enable safe and efficient UAM operations with these eVTOL aircraft. In this paper, we focus on solving one particular phase of the UAM operations, that is, UAM arrivals at a vertiport, by leveraging airspace design/configuration, trajectory optimization, eVTOL battery modeling, and arrival scheduling to support safe and efficient flight operations for on-demand, UAM arrivals.

In contrast to the small drones that can take off and land almost anywhere covered by UTM services, eVTOL vehicles in UAM operations need to take off from and land at specific ground infrastructures called vertiports. A vertiport is an airport for VTOL vehicles. It could range from a single landing pad on top of a parking structure to a larger building with multistory landing pads that could redefine the urban architecture and city planning [2]. When UAM traffic grows, one of the major emerging bottlenecks is expected to be the limited number of vertiports and landing pads. As such, UAM arrivals will become the most safety-critical flight phase due to limited resource of vertiport landing pads, high-density traffic in terminal airspace, frequent flight maneuvers, and low remaining battery energy for eVTOLs. Therefore, in this paper we propose a suite of mechanisms for tactical UAM arrival management, among which the rolling-horizon arrival scheduling algorithm enables a double-landing-pad vertiport to land peak-hour eVTOLs with less than 50 s average delay per aircraft.

The contribution of this paper is twofold. First, we propose a vertiport terminal area airspace design 13 with a double-landing-pad vertiport and multiple arrival routes. Second, based on this airspace structure, we develop a rolling-horizon optimization algorithm that sequences and schedules multiple eVTOLs arriving at the vertiport. Our algorithm extends existing arrival optimization models designed for commercial aviation [3–5]. The eVTOLs we consider are constrained by their remaining battery energy and their flight performance parameters. Our aim is to minimize the total eVTOL arrival delay at the vertiport. We formulate this problem as a rolling-horizon, mixed-integer linear program. We determine an optimal required time of arrival (RTA) for eVTOLs arriving at the vertiport. These RTAs are the decision variables in our optimization model, that is, the required time for the eVTOLs to arrive at the vertiport. Finally, we apply our sequencing and scheduling optimization algorithm in a case study on arrivals at a hexagonal vertiport network in Houston, TX. The performance of our algorithm is evaluated for different vertiport configurations. Our simulation results show that, during peak hours, at least two landing pads are needed to accommodate the demand. Moreover, we also show that during the peak hours, up to 50 s delay per eVTOL is expected, whereas during off-peak hours, less than 10 s delay per eVTOL is expected.

The remainder of this paper is organized as follows. In Sec. II we discuss existing literature on eVTOL operations. In Sec. III we present a model for eVTOLs arrival sequencing and scheduling at a double-landing-pad vertiport. In Sec. IV we present sequencing and scheduling results for an EHANG 184 arriving at a double-landing-pad vertiport. In Sec. VI we provide conclusions and recommendations for future work.

Received 11 July 2019; revision received 22 October 2019; accepted for publication 3 December 2019; published online 27 December 2019.

*M.Sc. Student, Department of Control and Operations, Faculty of Aerospace Engineering, Kluyverweg 1.

†Assistant Professor, Department of Control and Operations, Faculty of Aerospace Engineering, Kluyverweg 1.

‡Assistant Professor, Department of Aerospace Engineering, 2333 Howe Hall. Senior Member AIAA.

II. Related Work

Current UAM research efforts are mainly focused on the design of an urban airspace for UAM [2,6,7], on UAM demand forecasting [7,8], and on the design of the vehicles.

One of the most pressing operational challenges for near-terminal on-demand UAM operations is the sequencing and scheduling of arrivals because eVTOL flight time is constraint by the remaining life of their electric batteries, the capacity of vertiports is limited, and the operations do not follow a predefined arrival schedule. For commercial aviation, where the terminal area exhibits complex arrival trajectories [9], a significant amount of research has addressed the problem of aircraft arrival sequencing and scheduling at an airport [3–5,10,11]. However, none of these models consider the remaining flight time as a constraint, as is the case in this paper, where the eVTOL arrivals scheduling problem is restricted by the flight time supported by electric batteries. In fact, research focused on commercial aviation aims at optimizing the arrival process by minimizing the fuel consumption [12] or by optimally sequencing the arrival to avoid fuel shortage [13], whereas the electric battery flights supported by eVTOLs pose new battery-related constraints. Various aspects of eVTOL arrival procedures have been investigated in [14,15]. In [14] an eVTOL vehicle routing, departure, and arrival scheduling is developed such that minimum separation is ensured. Here, eVTOL traffic is integrated with existing air traffic. In our previous work [15] we propose an arrival sequencing and scheduling algorithm that minimizes eVTOL delay while considering limited battery power and limited, one-landing-pad vertiport capacity.

Existing literature regarding electric battery discharge models for aircraft is limited. In [16–18] battery modeling and predictions for electric winged aircraft are proposed based on flight testing. In these studies, voltage and state-of-charge (SOC) profiles are created based on a flight plan using an equivalent circuit model to check if the flight mission can be completed. Because we are not performing flight testing, in this paper we consider a simpler, theoretical battery model [19] that can support eVTOL operations.

This research extends the arrival scheduling models from previous work to a rolling-horizon, eVTOL arrivals sequencing and scheduling at a double-landing-pad vertiport. We analyze our proposed model using a 1-day operations demand corresponding to a hexagonal vertiport network in Houston, TX.

III. Model Formulation

In this section, we first introduce a generic airspace structure for eVTOL arrivals at a vertiport with two landing pads. Next, we propose an optimization model for a rolling-horizon eVTOL arrivals at a vertiport with two landing pads. In doing so, we make use of a flight dynamics model for eVTOLs equipped with one electric battery and a model for the SOC of an electric battery.

Lastly, we analyze our optimization model by means of an eVTOL arrival demand model corresponding to a use case of hexagonal vertiport network in Houston, TX. This use case and its operational concept are described in [20].

In this paper, we consider only eVTOL arrival operations and assume that the two landing pads are used for arrivals only. However, our scheduling model is generic and could be extended to departure operations or mixed operations with departures and arrivals. Another operational assumption is continuous descent approach plus a final vertical landing. This consideration is due to operational safety, to avoid vortex ring state, and energy efficiency [21]. Finally, our approach is applicable for other eVTOL aircraft types, as long as new flight dynamics and battery model are provided.

A. Airspace Structure for eVTOL Arrivals at a Vertiport

According to [20,22,23] and above assumptions, we consider eVTOLs arriving at a vertiport with two landing pads. We assume two arrival and two departure metering fixes [22] located on a radius, r, from the vertiport (see Fig. 1). The metering fixes are the entrance and exit "gates" to enforce time-based separation. The main use of the arrival approach fixes is to funnel traffic and, most important, to push the delay absorption to an area with lower traffic density, further away from the vertiport. We note, however, that the geometry in Fig. 1, that is, the location of the approach fixes on the circle of radius r around the vertiport and the values for R and r, does not affect the formulation of the scheduling model, but only the values of the time-to-fly to an approach fix and vertiport, which influence the numerical results of the scheduling model.

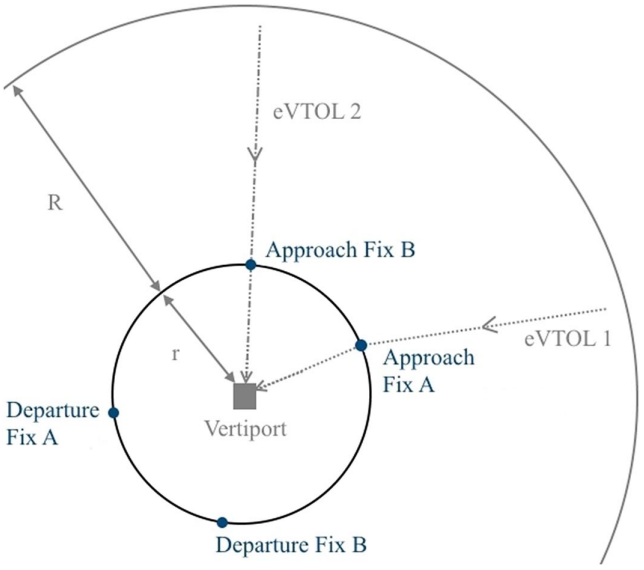

Fig. 1 Airspace structure for eVTOL arrivals at a vertiport with 2 landing pads—top view.

Arrivals are initiated on a radius, R, from the approach fixes. In this paper, we consider only two arrival fixes, referred to as approach fixes A and B. The distance between the arrival approach fixes is determined as follows. We assume that the final approach area is circular and has a radius of 400 m. Then the approach fixes are spaced around the vertiport by a quarter of the final approach area circumference. eVTOLs arriving through fix A (B) land at a corresponding landing pad A (B), independently of the arrivals at the other fix and landing pad. The arrival flow from approach fix A is separated by a distance, s, from the flow from approach fix B (see Fig. 2). Moreover, consecutive arrivals at an approach fix and its corresponding landing pad are separated by Δt_{sep} time units. The flights up to the approach fixes consist of a cruise phase followed by a continuous shallow descent phase (see Fig. 2). Continuous shallow descents are selected for energy efficiency and delay absorption [21]. After reaching one of the two approach fixes (see Fig. 2), an arriving eVTOL flies a horizontal flight segment of length d, followed by a vertical descent of altitude h.

The structure of the arrival airspace above considers the flight performances of EHANG 184 [23]. Taking into account a possible shallow descent for EHANG 184 up to the approach fixes, we consider $R = 3500$ m. We also assume a minimum separation $\Delta t_{\text{sep}} = 90$ s between consecutive arrivals to ensure a minimum lateral separation of 1000 ft or 305 m [20]. This also avoids that

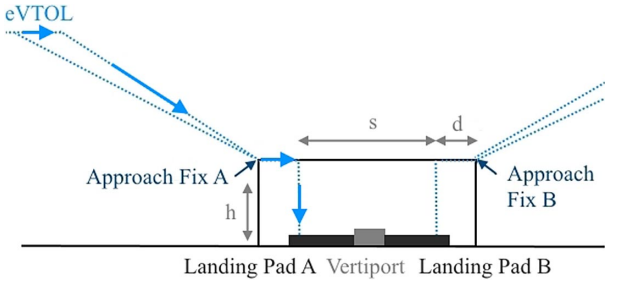

Fig. 2 Airspace structure for eVTOL arrivals at a vertiport with 2 landing pads–side view.

two or more eVTOLs are at the same time in the vertical flight phase. Moreover, it ensures that there is sufficient time for landing pad clearance.

The radius $r = 400$ m and $s = 530$ m follow from having $\Delta t_{\text{sep}} = 90$ s and an average eVTOL horizontal speed of 5.9 m/s during the final approach. The distance $d = 135$ m follows from the values assumed for r and s. Lastly, $h = 200$ m allows for a maximum eVTOL shallow descent from a cruise altitude of 500 m [23] and ensures clearance from high-rise buildings.

B. eVTOL Flight Dynamics Model

We consider the following flight dynamics model for EHANG 184 multirotor eVTOL [23], which is equipped with one electric battery:

$$P_r = P_i + P_a + P_c + P_f = 4 \cdot T \cdot v_i + T \cdot V \cdot \sin\alpha + 0.2 \cdot P_r \tag{1}$$

$$V = \sqrt{V_x^2 + V_h^2} \tag{2}$$

$$\alpha = \theta + \gamma = \theta + \arctan\left(\frac{V_x}{V_h}\right) \tag{3}$$

$$v_h = \sqrt{\frac{T_r}{2\rho\pi R^2}} \tag{4}$$

$$v_i = \frac{v_h^2}{\sqrt{(V \cdot \cos(\alpha))^2 + (V \cdot \sin(\alpha) + v_i)^2}} \tag{5}$$

where P_r, P_i, P_a, P_c, P_f are the required, induced, parasite, climb, and profile power, respectively, with $P_f = 0.2P_r$ [24]; V is the true airspeed with the vertical component V_x and the horizontal component V_h; $T, \alpha, \theta, \gamma$ are the thrust, the angle of attack, the pitch angle, and flight path angle, respectively; and also, v_i, v_h, R, T_r, ρ are the induced velocity, the induced velocity in hover, rotor radius, thrust per rotor, and the air density, respectively. Here, ρ is assumed to be equal to the international standard atmosphere density at sea level. We further assume that all rotors produce equal thrust. Thus, we assume an upper and lower rotor to produce equal thrust such that $T_r = (1/8)T$. Lastly, the induced velocity v_i in Eq. (5) follows from the momentum theory and the induced velocity in hover, denoted by v_h.

C. Electric Battery State-of-Charge

We consider the following model for the total electric power demand, P_d [18,19]:

$$P_d = \text{SF} \cdot \frac{1}{\eta_P}\frac{1}{\eta_e} P_r \tag{6}$$

where SF = 1.5 is a safety factor to account for potential adverse weather conditions and the need for emergency diversion, η_P is the rotor efficiency ($\eta_P = 0.7652$), and η_e is the mechanical efficiency ($\eta_e = 0.85$). We further consider the following model [19] for the battery SOC demand during a flight phase k that starts at time t_0^k and ends at time t_f^k, $1 \le k \le 4$, where $k = 1$ corresponds to the cruise phase, $k = 2$ corresponds to the shallow descent phase, $k = 3$ corresponds to the horizontal final approach, and $k = 4$ corresponds to the vertical final approach:

$$I(k) = \frac{P_d(k)}{V_n} \tag{7}$$

$$\text{SOC}(k) = \frac{I(k) \cdot (t_f^k - t_0^k)}{3600 \cdot Q} \tag{8}$$

$$\text{SOC} = \sum_{k=1}^{4} \text{SOC}(k) \tag{9}$$

where $I(k)$ is the total current of all battery cells during flight phase k, $1 \le k \le 4$; V_n is the nominal battery voltage; and Q is the battery capacity. The battery is assumed to be empty if it reaches a 10% SOC, to prevent it from deep discharge. We use this battery model and the flight dynamics model in Sec. III.B to limit the latest possible landing time RTA_l. This hard constraint ensures that each aircraft lands before its SOC drops below 10%.

D. Rolling-Horizon eVTOL Arrival Sequencing and Scheduling at a Vertiport

Using the airspace structure in Sec. III.A, the flight dynamics model for an eVTOL in Sec. III.B, and the eVTOL battery model in Sec. III.C, in this section we propose an optimal, rolling-horizon sequencing and scheduling algorithm for eVTOL arrivals at a vertiport. We also take into account the possibility for eVTOLs to hover at a distance $R + r$ away from the vertiport. Here, hovering is seen as an additional possibility to impose delay on eVTOLs when the arrival rate is larger than the landing rate of the eVTOLs at the vertiport, that is, the delay imposed on eVTOLs is too large to be absorbed by means of shallow descent. The objective of this optimization model is to minimize the total time deviation of arriving eVTOLs from their preferred time of arrival. Next we define the preferred eVTOL times of arrival.

First, given the airspace structure in Sec. III.A and the eVTOL flight dynamics in Sec. III.B, we determine, for a given RTA at the vertiport, an optimal eVTOL arrival trajectory with respect to energy consumption. These optimal arrival trajectories are computed using the GPOPS-II software [25]. For a given RTA, the output of GPOPS-II is an optimal eVTOL arrival trajectory, which is defined by the state variables (V_x, V_h, altitude, and distance), the control variables (T and θ), and the total energy required to fulfill the trajectory.

Next, we use the GPOPS-II output to determine the required power P_r at each flight phase k, $1 \le k \le 4$, of the eVTOL arrival trajectory (see also Sec. III.B). Further, P_r is used to determine the battery power demand P_d and the SOC demand for the eVTOL battery (see Sec. III.C). We determine a feasible set of RTAs based on the remaining SOC of the eVTOLs, the minimum required SOC to reach the vertiport at these RTAs, and the flight performance of the eVTOLs. The minimum RTA in the feasible set corresponds to the earliest possible time that the eVTOL can arrive at the vertiport. The maximum RTA in the feasible set is determined by the SOC of the eVTOL battery. The RTA obtained with the minimum energy consumption, which we refer to as the estimated time of arrival (ETA), is the preferred arrival time of an eVTOL at the vertiport.

Having obtained a set of feasible RTAs for arriving eVTOLs, we next introduce a rolling-horizon optimization model that sequences and schedules a set of G eVTOLs arriving at a vertiport such that the total time deviation from their ETAs, that is, $\sum_{i \in G} |\text{RTA}_i - \text{ETA}_i|$, is minimized. The rolling-horizon [5,26] consists of planning periods of 15 min and a total planning horizon of 30 min, that is, 2 planning periods (see Fig. 3). In each planning horizon, we find the eVTOL RTAs that result in a minimal total time deviation from their ETAs. We freeze the RTAs of the eVTOLs in the first planning period, that is, during the first 15 min. We also save the last RTA in this period, for each landing pad $\text{RTA}_{\text{last},lp}(i)$, $i \in \{A, B\}$. We further shift the planning horizon by 15 min and optimize the arrival time of the remaining

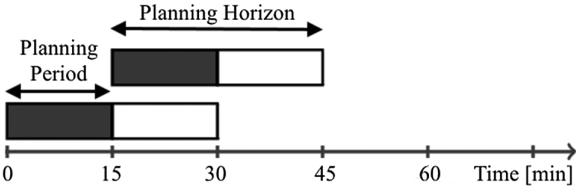

Fig. 3 Rolling-horizon for eVTOL sequencing and scheduling.

eVTOLs. We also ensure minimum separation between the time of the last eVTOL arrival in the previous planning period and the first eVTOL arrival in the next planning period.

1. Decision Variables

We optimize the values of the following decision variables:

$$a^p = \begin{cases} 1, & \text{if eVTOL } p \text{ flies through approach fix } A, \\ 0, & \text{if eVTOL } p \text{ flies through approach fix } B, \end{cases} \quad \forall\ p \in G,$$

$$z^{pq} = \begin{cases} 1, & \text{if eVTOL } p \text{ and eVTOL } q \text{ fly through the same approach fix,} \\ 0, & \text{otherwise} \end{cases} \quad \forall\ p, q \in G,$$

$$s^{pq} = \begin{cases} 1, & \text{if eVTOL } p \text{ arrives prior to eVTOL } q, \\ 0, & \text{otherwise} \end{cases} \quad \forall\ p \in G, q \in [p-K, p+K], p \neq q, \quad \text{where } K \in \mathbb{N}^+ \text{ is}$$

the maximum number of position shifts from the first-come-first-served (FCFS) arrival sequence [27].

$\Delta t_e^p =$ Amount of time eVTOL p is scheduled beforeits $\text{ETA}^p(i),\ i \in \{A, B\}$, i.e., $\text{ETA}^p(i) - \text{RTA}^p(i), \quad \forall\ p \in G, \Delta t_e^p \geq 0$

$\Delta t_l^p =$ Delay assigned to eVTOL p in shallow descent, that is, amount of time eVTOL p is scheduled after its $\text{ETA}^p(i), i \in \{A, B\},$ i.e., $\text{RTA}^p(i) - \text{ETA}^p(i), \quad \forall\ p \in G, \Delta t_l^p \geq 0$

$\Delta t_{l,h}^p =$ Delay assigned to eVTOL p in hover at distance $R + r$ from the vertiport, that is, amount of time eVTOLp is scheduled after its $\text{ETA}^p(i), i \in \{A, B\},$ i.e., $\text{RTA}^p(i) - \text{ETA}^p(i), \quad \forall\ p \in G, 0 \leq \Delta t_{l,h}^p \leq \Delta t_{l,h,\max}^p$

where $\Delta t_{l,h,\max}^p$ is determined from the remaining battery SOC.

2. Objective Function

The total time deviations from the ETAs of the eVTOLs arriving at the vertiport are minimized, that is,

$$\min \sum_{p \in G} c_e^p \cdot \Delta t_e^p + c_l^p \cdot \Delta t_l^p + c_{l,af}^p \cdot a^p \cdot (\Delta t_{l,A}^p - \Delta t_{l,B}^p) + c_{l,h}^p \cdot \Delta t_{l,h}^p, \quad \text{where} \tag{10}$$

$$\Delta t_{l,i}^p = \max(0, (\text{ETA}^p(i) + T_t^p(i) - \text{ETA}^p(j) - T_t^p(j))) \quad \forall\ i, j \in \{A, B\},\ i \neq j \tag{11}$$

The first term in Eq. (10) penalizes the amount of time eVTOLs arrive at the vertiport before their ETA. The second term penalizes the delay assigned to eVTOLs in shallow descent. The third term penalizes the additional flight time resulting from selecting an approach fix i, $i \in \{A, B\}$, which needs more time to reach, that is, requires a longer arrival trajectory, than the other approach fix j, $j \in \{A, B\}$, $i \neq j$. The delay resulting from choosing an approach fix, that is, $\Delta t_{l,i}^p$, $i \in \{A, B\}$, is calculated using Eq. (11), where $T_t^p(i)$ is the flight time between the approach fix i, $i \in \{A, B\}$, and the vertiport. The fourth term penalizes the time the eVTOL spends hovering at distance $R + r$ from the vertiport. Further, $c_e^p, c_l^p, c_{l,af}^p, c_{l,h}^p$ are the cost coefficients corresponding to the four penalty terms above, where $c_e^p, c_l^p, c_{l,af}^p, c_{l,h}^p$ are derived from the power required to absorb the assigned time deviation of an eVTOL from its ETA.

3. Constraints

We require the following set of constraints to be satisfied:

$$s^{pq} + s^{qp} = 1, \quad \forall\ p, q \in G \tag{12}$$

$$z^{pq} = z^{qp}, \quad \forall\ p, q \in G \tag{13}$$

$$z^{pq} \geq a^p + a^q - 1, \quad \forall\ p, q \in G, p \neq q \tag{14}$$

$$z^{pq} \geq -a^p - a^q + 1, \quad \forall\ p, q \in G, p \neq q \tag{15}$$

$$z^{pq} \leq \frac{1}{2}a^p - \frac{1}{2}a^q + 1, \quad \forall\ p, q \in G, p \neq q \tag{16}$$

$$z^{pq} \leq -\frac{1}{2}a^p + \frac{1}{2}a^q + 1, \quad \forall\ p, q \in G, p \neq q \tag{17}$$

$$\text{RTA}_e^p \leq \text{RTA}^p \leq \text{RTA}_l^p, \quad \forall\ p \in G \tag{18}$$

$$\text{RTA}^p \geq \text{RTA}^q + \Delta t_{\text{sep}}^{qp} \cdot z^{qp} - M^{pq} \cdot s^{pq}, \quad \forall\ p, q \in G, p \neq q \tag{19}$$

$$\text{RTA}^p(i) \geq \text{RTA}^q(i) + \Delta t_{\text{sep}}^{qp} \cdot z^{qp} - M^{pq} \cdot s^{pq}, \quad \forall\ p, q \in G, p \neq q, i \in \{A, B\} \tag{20}$$

in which

$$\text{RTA}_e^p = a^p \cdot \text{RTA}_{e,lp}^p(A) + (1 - a^p) \cdot \text{RTA}_{e,lp}^p(B) \tag{21}$$

$$M^{pq} = \text{RTA}_l^q + \Delta t_{l,h,\max}^p + \Delta t_{\text{sep}}^{qp} - \min(\text{RTA}_{e,lp}^p(A), \text{RTA}_{e,lp}^p(B)) \tag{22}$$

$$\text{RTA}_{e,lp}^p(i) = \max(\text{RTA}_{\text{last},lp}(i) + \Delta t_{\text{sep}}^{pq}, \text{RTA}_e^p(i) + T_t^p(i)), \quad \forall\ i \in \{A, B\} \tag{23}$$

$$\text{RTA}^p = a^p \cdot (\text{RTA}^p(A) + T_t^p(A)) + (1 - a^p) \cdot (\text{RTA}^p(B) + T_t^p(B)) \tag{24}$$

$$\text{RTA}^p(i) = \text{ETA}^p(i) + \Delta t_l^p - \Delta t_e^p + \Delta t_{l,h}^p, \quad \forall\ i \in \{A, B\} \tag{25}$$

Constraint (12) ensures that either eVTOL p follows eVTOL q or eVTOL q follows eVTOL p. Equation (13) ensures that if eVTOL p

and q go through the same approach fix and to the same landing pad, the reverse is also true. Equations (14) and (15) further define $z^{pq} = 1$ if both eVTOL p and q use approach fix A and B, respectively. Equations (16) and (17) define $z^{pq} = 0$ if eVTOLs p and q fly through different approach fixes. The feasible set of RTAs for landing at the vertiport is described in Eq. (18). The latest RTA_l^p results from the battery model (see Sec. III.C), whereas the earliest possible time of arrival RTA_e^p is computed by Eq. (21). Here, $\text{RTA}_{e,lp}^p(i)$ is the earliest possible landing time of eVTOL p arriving through approach fix i and thus at landing pad i, $i \in \{A, B\}$. This is derived from the flight performance model (see Sec. III.B). Equations (19) and (20) ensure a time-based separation of at least $\Delta t_{\text{sep}}^{qp}$ only if eVTOL p follows eVTOL q at the same approach fix and, thus, the same landing pad. We consider variable M^{pq}, defined in Eq. (22), which ensures that the time separation between two eVTOLs is enforced only when $s^{pq} = 0$, that is, when eVTOL p arrives at the vertiport after eVTOL q. Equation (23) shows the earliest possible time to arrive at the vertiport based on the last eVTOL arrival time, $\text{RTA}_{\text{last},lp}$, in the previous planning period. Equations (24) and (25) define the RTA for eVTOL p at the selected vertiport landing pad and at approach fix A or B, respectively.

E. eVTOL Arrival Demand Model

We consider the eVTOL arrival demand model introduced in [8], where a prediction for an eVTOL arrival demand distribution over a day is provided for the hub vertiport in an envisioned hexagonal vertiport network of Houston, TX. In [8], the distribution of arrivals is determined as the sum of 3 normal distributions: $N(8, 2)$ and $N(16, 2)$ corresponding to commuter rush hour peaks at 8:00 a.m. and 4:00 p.m., respectively, and $N(12, 6)$ corresponding to daytime commuter travel. The obtained distribution (see Fig. 4) is normalized to a cumulative distribution and scaled by coefficient $M_4 = 8500$ [8].

Using the probability distribution function in [8] for eVTOL arrivals at the hub vertiport, we estimate $\lambda(t)$, the number of arrivals in hour t, $t \in \{0, 1, \ldots, 24\}$. Further, we consider an inhomogeneous Poisson process with rate $\lambda(t)$ to generate eVTOL interarrival times at the vertiport. Moreover, based on the hexagonal vertiport network structure in [8], we assume that the eVTOLs start their arrival trajectory from one of 6 equally spaced, origin points on a circle of radius $R + r$ (see Fig. 5). Each eVTOL has probability 1/6 of originating from one of the 6 origin points on the circle.

Now, let an eVTOL $p + 1$ arriving at an approach fix i, $i \in \{A, B\}$, be preceded by eVTOL p. Then, the expected time of arrival of eVTOL $p + 1$ at an approach fix i, $\text{ETA}(i)^{p+1}$, is determined in Eq. (26), where S is the interarrival time between eVTOL $p + 1$ and eVTOL p, and $\Delta t_{l,i}^p$ is the additional flight time due to selecting approach fix i, which results in a longer arrival trajectory than selecting the other approach fix [see also Eq. (11)].

$$\text{ETA}(i)^{p+1} = \text{ETA}(i)^p + S + \Delta t_{l,i}^p \tag{26}$$

where $S \sim \exp(\lambda(t))$, $i \in \{A, B\}$.

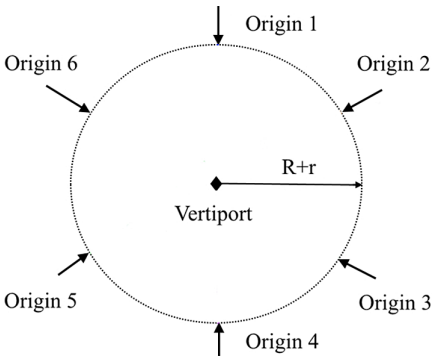

Fig. 5 Origin points for eVTOL arrivals at a hub vertiport.

Lastly, we assume that the initial SOC of an eVTOL p follows a normal distribution $N(30, 5)$, where a mean initial SOC battery of 30% allows for all trajectories with an RTA in the feasible set of RTAs (see Sec. III.D) to be fulfilled.

IV. Results

In this section we present the arrival sequencing and scheduling results for an EHANG 184 [23]. In Sec. IV.A we illustrate the energy consumption achieved by EHANG 184 for various RTAs and shallow descents. In Sec. IV.B we show the arrival delay for EHANG 184 for a rolling-horizon arrival sequencing and scheduling for 1 day of operations. In Sec. IV.C we discuss the distribution of EHANG 184 delays based on Monte Carlo simulation of a 1-day operations demand.

A. Energy-Optimal Arrival Trajectory for a Single eVTOL

In this section we determine, using the GPOPS-II trajectory optimizer and the flight dynamics model in Sec. III.B, the energy optimal arrival trajectories for a given set of RTAs at a given approach fix. The cruise phase is performed at 500 m altitude and 27.8 m/s cruise speed [23]. The eVTOL arrival scheduling and sequencing is initiated at $R + r = 3900$ m distance from the vertiport (see Sec. III.A). A shallow descent is initiated between 3400 and 1000 m from the vertiport at a constant horizontal velocity $V_h = 5.9$ m/s and variable vertical velocity V_x. After passing the approach fix, a horizontal flight phase is executed at velocity $V_h = 5.9$ m/s and a vertical flight phase at velocity $V_x = 2.9$ m/s.

Figure 6 shows the energy-optimal eVTOL arrival trajectories for given RTAs at the approach fix, RTA_{af}. For a large RTA_{af}, the eVTOLs spend this large time flying a more shallow descent. An $\text{RTA}_{af} = 165$ s is the shortest possible time to reach an approach fix, given the flight performance of EHANG 184 [23]. For 165 s $\leq \text{RTA}_{af} \leq$ 525 s, the eVTOL is required to arrive at the double-landing-pad vertiport at 262 s $\leq RTA \leq$ 622 s because the flight time between the approach fix and vertiport is 97 s. A trajectory with $\text{RTA}_{af} = 165$ s also corresponds to the minimum energy required to reach the approach fix. This trajectory with

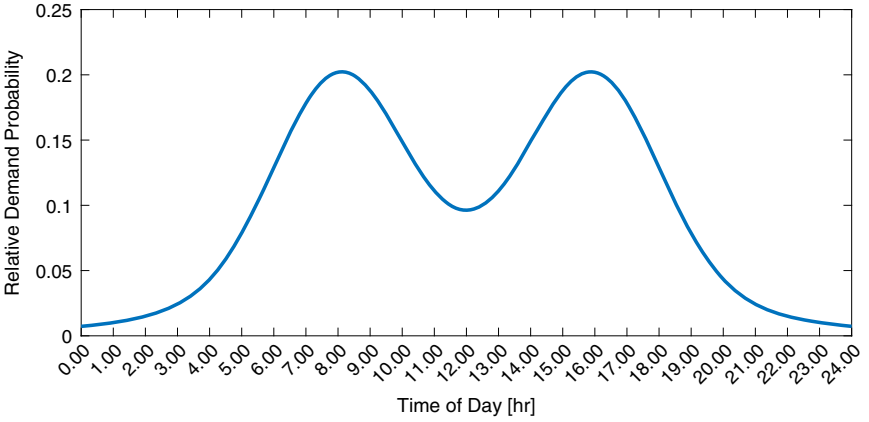

Fig. 4 Demand probability distribution function for eVTOL arrivals at a hub vertiport [8].

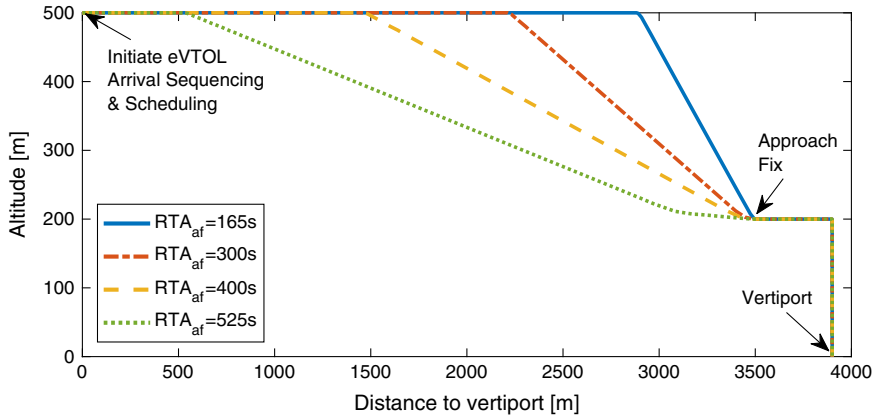

Fig. 6 EHANG 184 energy-optimal eVTOL arrival trajectory for different RTAs to approach fix.

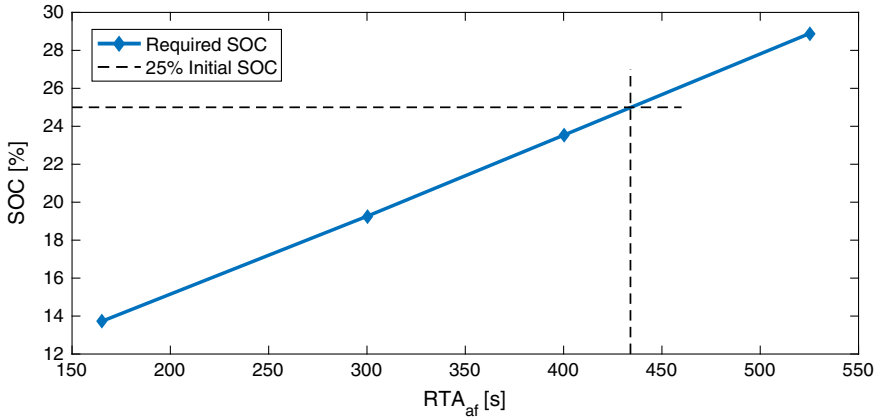

Fig. 7 Required SOC for different RTAs at approach fix.

$\text{RTA}_{af} = 165$ s is used as a baseline trajectory to determine the eVTOLs ETAs at the vertiport, which are an input for the sequencing and scheduling model.

Figure 7 shows the SOC required to perform each of the trajectories in Fig. 6, based on the battery model in Sec. III.C. We assume a battery capacity $Q = 5000$ Ahr and a nominal voltage $V_n = 12$V. Figure 7 shows, for instance, that for a remaining SOC $= 25\%$, the latest RTA at the approach fix is $\text{RTA}_{af} = 434$ s. Thus, the maximum RTA at the vertiport is RTA $= 531$s.

B. Rolling-Horizon Arrival Sequencing and Scheduling for a 1-Day eVTOL Arrival Demand

In this section we present the results of the rolling-horizon EHANG 184 arrival sequencing and scheduling optimization model. We run the optimization algorithm at the current time within a certain look-ahead planning period such as 5 and 10 min (see Table 1). After we calculate the RTAs for the flights in the current planning horizon, we fix the RTAs and sequencing obtained up to this moment and move to next planning horizon. Next, we consider the new eVTOL arrivals, and run the optimization algorithm again. We assume 1 day of operations demand, as introduced in Sec. III.E.

Table 1 Computational time for the rolling-horizon eVTOL arrival sequencing and scheduling problem

Length planning period, min	5	10	15	20
Average computational time per planning horizon, s	5.7	76	190	510

For the eVTOL arrival sequencing and scheduling optimization model, we consider $c_e^p = 0$, $c_l^p = 28$, $c_{l,af}^p = 36$, and $c_{l,h}^p = 42$, where $c_l^p = 28$ is the energy differential of a shallow descent trajectory that requires one additional second to be flown, that is, $(\Delta E/\Delta t) = 28$ kW; $c_{l,af}^p = 36$ is the power required to fly at cruise altitude and velocity; and $c_{l,h}^p = 42$ is the power required to hover. Lastly, $c_e^p = 0$ since, for EHANG 184, the most energy-efficient trajectory, after using GPOPS-II, also corresponds to the earliest possible arrival time at the approach fix, that is, $\text{RTA}_{af} = 165$ s. We also assume $K = 2$ [27].

Figure 8 shows eVTOL arrivals over 1 day of operations, which are generated based on the demand model [8] in Sec. III.E.

We compared our arrival sequencing and scheduling algorithm with a baseline heuristic algorithm called first-come-first-serve (FCFS). In Figs. 9 and 10, we can observe that our algorithm dominates the FCFS through a 24 h period in both reducing average delay and maximum delay. In air traffic control, the FCFS algorithm is a commonly used heuristic to mimic human controller's tactical decision-making process. Specifically, in this application, the FCFS logic tries to first schedule the eVTOL aircraft to the minimum ETA between the ETA to fix A and the ETA to fix B. If this minimum ETA is the ETA to fix A and fix A is available (satisfying time separation constraint), then we schedule the eVTOL to fix A. If the minimum ETA is the ETA to fix B and fix B is available, then we schedule it to fix B. If the minimum ETA is the ETA to fix A and fix A is not available, but fix B is available, then we schedule it to fix B. If the minimum ETA is the ETA to fix B and fix B is not available, but fix A is available, then we schedule it to fix A. In all cases, if the RTA exceeds the RTA upper bound according to the SOC, then we do not schedule this eVTOL. This corresponds to the case when, for instance, the eVTOL is redirected to another landing pad.

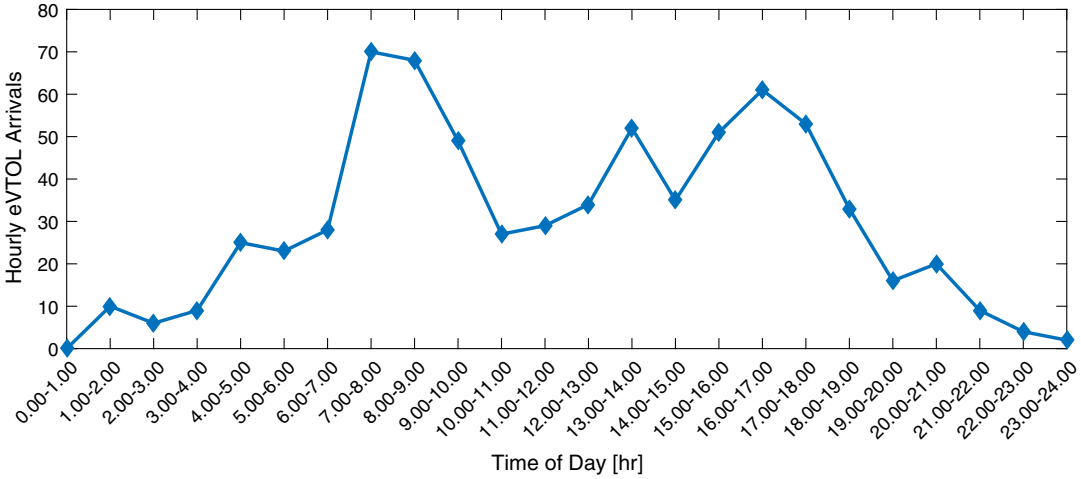

Fig. 8 Hourly eVTOL arrivals at the hub vertiport.

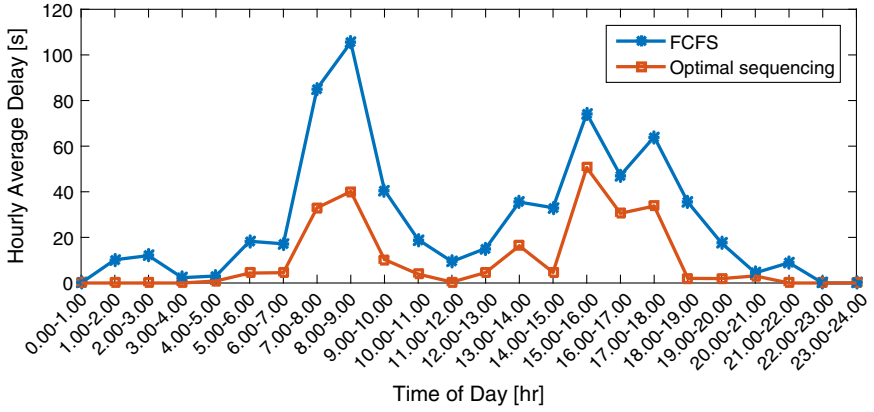

Fig. 9 Average eVTOL delay at the vertiport for 1 day.

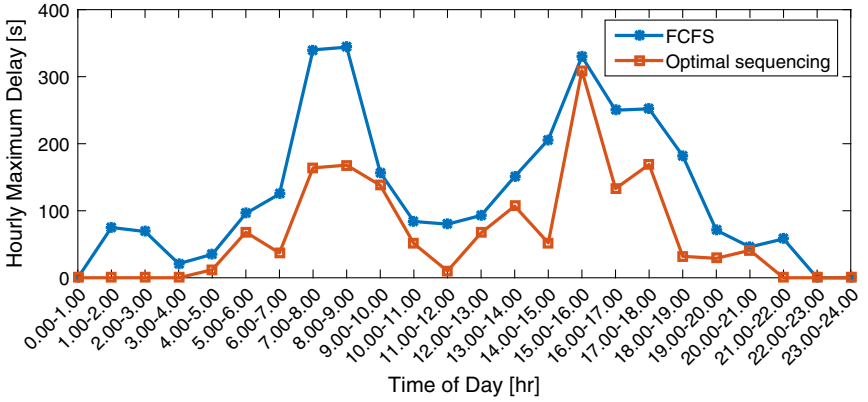

Fig. 10 Hourly maximum eVTOL delay at a double-landing-pad vertiport.

Figure 9 shows the average delay, that is, (RTA − ETA), imposed on eVTOLs arriving at the vertiport. Let us focus on discussing the result of our scheduling algorithm (the orange curve). In accordance to the demand peaks in Fig. 8, the eVTOLs start to experience delays from early morning at 7:00 a.m. until 9:00 a.m., with the highest average delay of 40 s. The eVTOL delays decrease significantly after 10:00 a.m. From 3:00 p.m., eVTOLs start experiencing higher delays again, with a highest average delay of 50 s. Figure 10 shows the maximum amount of delay that eVTOLs experience when arriving at the vertiport. Again, the highest delays occur around the peak demand hours, between 8:00 a.m. and 9:00 a.m. (168 s) and between 3:00 p.m. and 4:00 p.m. (309 s).

Table 1 shows both the computational time required to sequence and schedule, using a rolling-horizon approach, 1 day of operations, as well at the computational time for one planning horizon only. The results are obtained using CPLEX LP Solver extension of MATLAB on a computer with Intel CORE i7 processor. Table 1 shows that the required computational time is significantly high for a planning horizon of 15 min or more. The use of short planning periods is, however, suitable for on-demand UAM, where demand for eVTOLs occurs ad-hoc during the day.

Figure 11 shows the impact of the minimum time separation between consecutive arrivals at the vertiport on the delay experienced by the eVTOLs. Increasing the time separation from 90 to 100 s

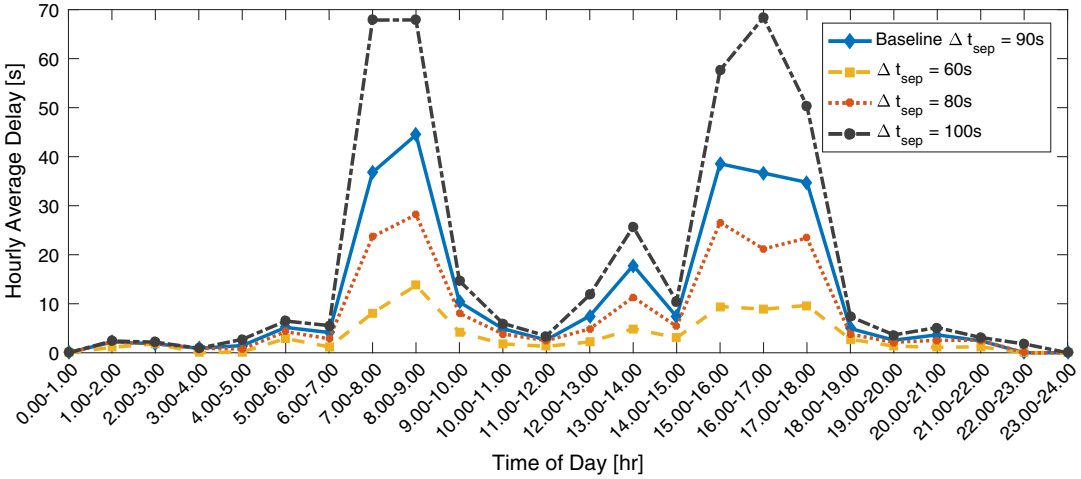

Fig. 11 Average eVTOL delay at a double-landing-pad vertiport—various minimum time separations.

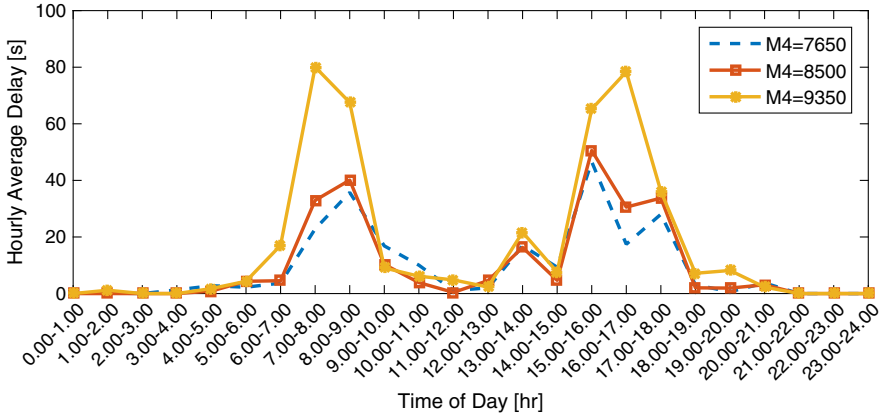

Fig. 12 Average eVTOL delay at a double-landing-pad vertiport—various coefficients of the eVTOL demand model.

shows that, during peak demand hours around 8:00 a.m. and 4:00 p.m., the eVTOL delays increase by up to 75%. In contrast, a time separation of 60 s results in eVTOL delay of at most 10 s, even during peak demand hours. Thus, designing eVTOLs for low time separation requirements is beneficial for on-time operations.

In Fig. 12, the performance of the scheduling model in terms of hourly expected delays is shown for different scaling coefficient M_4 of the eVTOL demand (see Sec. III.E). The results show that, for an increase of 10% in the scaling coefficient, that is, $M_4 = 9350$, the expected delay during peak hours is almost double, compared with the baseline demand model with $M_4 = 8500$. The impact on delay is less for a decrease of 10% in the scaling coefficient, that is, $M_4 = 7650$.

C. Monte Carlo Simulation of eVTOL Operations Demand

We perform a Monte Carlo simulation of the demand of eVTOL operations (see Sec. III.E [8]) and evaluate the distribution of eVTOL delays. In particular, we consider that eVTOLs arrive at an area of radius 3900 m around the vertiport according to a stochastic process. Also, the initial SOC of the batteries is assumed to follow a Gaussian distribution. For computational purposes, we evaluate two demand periods only: 1) a peak demand period between 7:30 a.m. to 8:30 a.m. and 2) an off-peak demand period during noon time, from 11:30 a.m. to 12:30 p.m., when half as many eVTOL arrivals as in the peak period are expected to occur (see Fig. 4).

Figures 13 and 14 show that in off-peak periods, up to 94% of the arriving eVTOLs experience at most 1 min delay. However, in the peak period, only 72% of the arriving eVTOLs experience at most 1 min delay, with 24% of the eVTOLs having a delay of 1–3 min.

Figure 15 shows the distribution on the eVTOL arrival delays when considering a single- and a double-landing-pad vertiport, respectively. The eVTOL arrival sequencing and scheduling optimization model for a vertiport with one landing pad has been considered in [15]. The model in [15] has been further extended by considering a rolling-horizon approach to determine an optimal eVTOL arrival schedule. Moreover, the model has been extended with the possibility for eVTOLs to hover at a distance $R + r$ from the vertiport.

Figures 14 and 15 show that, during off-peak periods, having a double-landing-pad vertiport results in 94% of the arriving eVTOLs having at most 1 min delay. However, having a single-landing-pad vertiport results only in 56% of the arrivals experiencing at most 1 min delay, with 31% of the arrivals having a delay of 1–4 min. We note that for the peak hour 7:30 a.m. to 8:30 a.m., due to the high number of eVTOL arrivals, a single landing pad cannot accommodate the demand; thus we have not considered this case for simulation.

V. Discussion

This paper addresses the eVTOL arrival sequencing and scheduling at a vertiport terminal airspace such that the arrival delays are minimized. We consider potential shallow descent approaches to induce arrival delay. In turn, we generate RTA for the incoming aircraft to enforce such delays. We envision that this arrival management model will complement predeparture planning/scheduling models and strategic air traffic flow management models, while supporting safe and efficient UAM operations.

In practice, we expect additional challenges for the eVTOL arrival process. First, the arrival process is impacted by the capacity of the

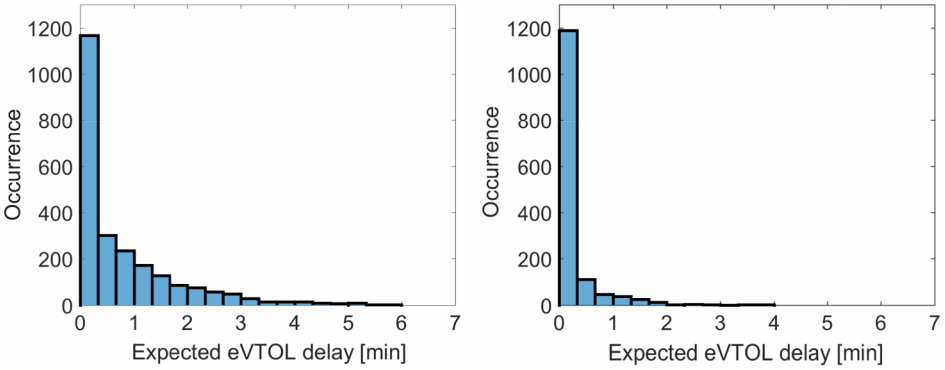

a) Peak hour 7:30AM-8:30AM b) Off-peak hour 11:30AM-12:30PM

Fig. 13 Distribution of eVTOL delay for eVTOLs arriving at a double-landing-pad vertiport.

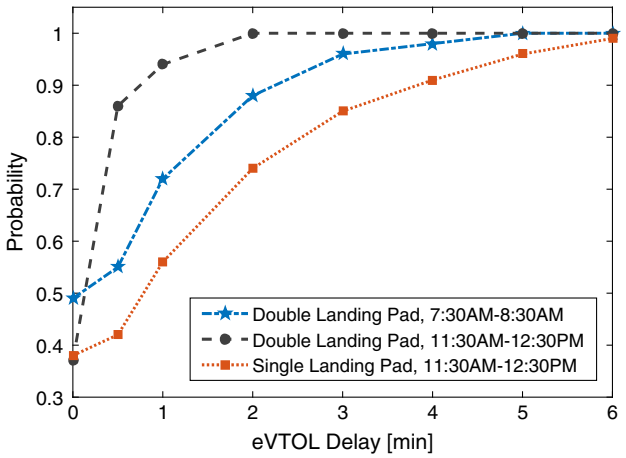

Fig. 14 Cumulative distribution function for eVTOL delay.

vertiport and, in particular, by the eVTOL turnaround requirement. Although we consider arrival management to be one of the main priorities for UAM operations, due to eVTOL battery constraints and envisioned high traffic densities in the terminal area, it remains a challenge to analyze together the arrival, turnaround, and departure processes at a vertiport.

Second, further analysis of the potential demand for eVTOL operations throughout a day is needed to assess arrival scheduling algorithms. In particular, dedicated arrival heuristics should be developed to account for extreme demand values. For instance, in our paper we analyzed the FCFS heuristic, which is commonly used for arrival sequencing and scheduling of commercial aviation. Lastly, the design of contingency plans, such as, for instance, eVTOL vectoring or hovering, should be investigated together with arrival management algorithms.

VI. Conclusions

In this paper, a double-landing-pad vertiport where on-demand eVTOLs arrive is considered. An optimal, rolling-horizon eVTOL sequencing and scheduling algorithm is proposed such that time deviations from a preferred arrival time are minimized. The optimization problem is formulated as a mixed-integer linear program with constraints regarding the minimum time separation, electrical battery discharge, and vehicle dynamics. The discharge battery model, in particular, makes this arrival scheduling algorithm specially designed for eVTOL operations. The sequencing and scheduling problem is solved using a rolling-horizon approach for 1 day of operations, where the demand for operations corresponds to a hexagonal vertiport network in Houston, TX. Our proposed sequencing and scheduling algorithm has arrival route selection capability. The algorithm outputs landing time slots (or RTAs) for all arriving eVTOLs to achieve minimum total delay. The distribution of delays imposed on the arriving eVTOLs at the vertiport is determined. It is shown that a double-landing-pad vertiport is able to accommodate the demand in both off-peak and peak hours, with eVTOLs average delays up to 50 s in peak hours.

Future work will include 1) exploring other heuristics to achieve near-real-time, suboptimal solutions under high eVTOL demands; 2) design of terminal airspace and estimation of vertiport capacities; 3) accounting for uncertainties with respect to the eVTOL flight performance; and 4) investigating other delay absorption concepts

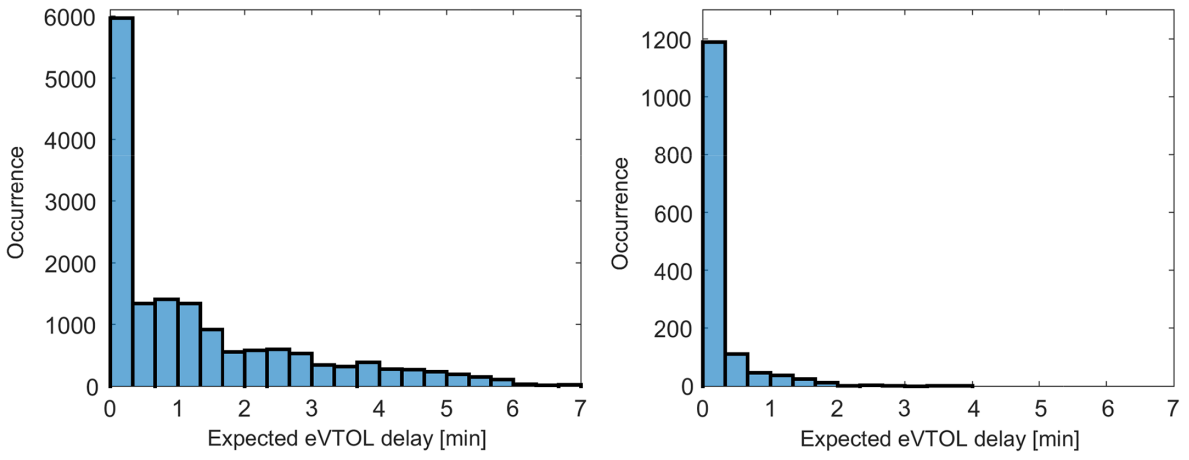

a) Single landing pad vertiport b) Double landing pad vertiport

Fig. 15 Distribution of eVTOL delay during an off-peak hour 11:30 a.m. to 12.30 p.m.

such as ground delay at the departure vertiport, hovering, and vectoring.

References

[1] Polaczyk, N., Trombino, E., Wei, P., and Mitici, M., "A Review of Current Technology and Research in Urban On-Demand Air Mobility Applications," *8th Biennial Autonomous VTOL Technical Meeting and 6th Annual Electric VTOL Symposium*, Mesa, Arizona, 2019.

[2] "Fast-Forwarding to a Future of On-Demand Urban Air Transportation," Uber Elevate Tech. Rept., Uber Elevate Whitepaper, 2016, uber.com/elevate/whitepaper [accessed 10 Dec. 2019].

[3] Guérert, C., Prins, C., and Sevaux, M., *Applications of Optimization with XPress-MP*, Dash Optimization, Eyrolles, Paris, 2000, pp. 82–103, Chap. 7.

[4] Pawelek, A., Lichota, P., Dalmau, R., and Prats, X., "Arrival Traffic Synchronisation with Required Time of Arrivals for Fuel-Efficient Trajectory," *Proceedings of the 17th ATIO-AIAA Aviation Technology, Integration, and Operations Conference*, 2017, pp. 1–14.

[5] Hu, X., and Chen, W., "Genetic Algorithm Based on Receding Horizon Control for Arrival Sequencing and Scheduling," *Engineering Applications of Artificial Intelligence*, Vol. 18, No. 5, 2005, pp. 633–642. https://doi.org/10.1016/j.engappai.2004.11.012

[6] Vascik, P., and Hansman, J., "Constraint Identification in On-Demand Mobility for Aviation Through an Exploratory Case Study of Los Angeles," *Proceedings of 17th AIAA Aviation Technology, Integration, and Operations Conference*, 2017, pp. 1–25.

[7] Alonso, J., Arneson, H., Melton, J., Vegh, M., Walker, C., and Young, L., "System-of-Systems Considerations in the Notional Development of a Metropolitan Aerial Transportation System," Tech. Rept., Stanford Univ. and NASA Ames Research Center, 2017, https://nari.arc.nasa.gov/sites/default/files/Young_HopperII_NASA_TM15K.pdf [accessed 10 Dec. 2019].

[8] Kohlman, L., and Patterson, M., "System-Level Urban Air Mobility Transportation Modeling and Determination of Energy-Related Constraints," *Proceedings of Aviation Technology, Integration, and Operations Conference*, AIAA Paper 2018-3677, 2018.

[9] Olive, X., and Morio, J., "Trajectory Clustering of Air Traffic Flows Around Airports," *Aerospace Science and Technology*, Vol. 84, Jan. 2019, pp. 776–781. https://doi.org/10.1016/j.ast.2018.11.031

[10] Bennell, J. A., Mesgarpour, M., and Potts, C. N., "Airport Runway Scheduling," *4OR—A Quarterly Journal of Operations Research*, Vol. 9, No. 2, 2011, p. 115–138. https://doi.org/10.1007/s10288-011-0172-x

[11] Ozgur, M., and Cavcar, A., "0–1 Integer Programming Model for Procedural Separation of Aircraft by Ground Holding in ATFM," *Aerospace Science and Technology*, Vol. 33, No. 1, 2014, pp. 1–8. https://doi.org/10.1016/j.ast.2013.12.009

[12] Andreeva-Mori, A., Suzuki, S., and Itoh, E., "Rule Derivation for Arrival Aircraft Sequencing," *Aerospace Science and Technology*, Vol. 30, No. 1, 2013, pp. 200–209. https://doi.org/10.1016/j.ast.2013.08.004

[13] Wu, Y., Sun, L., and Qu, X., "A Sequencing Model for a Team of Aircraft Landing on the Carrier," *Aerospace Science and Technology*, Vol. 54, July 2016, pp. 72–87. https://doi.org/10.1016/j.ast.2016.04.007

[14] Bosson, C., and Lauderdale, T., "Simulation Evaluations of an Autonomous Urban Air Mobility Network Management and Separation Service," *Proceedings of Aviation Technology, Integration, and Operations Conference*, AIAA Paper 2018-3365, 2018.

[15] Kleinbekman, I., Mitici, M., and Wei, P., "eVTOL Arrival Sequencing and Scheduling for On-Demand Urban Air Mobility," *37th AIAA/IEEE Digital Avionics Systems Conference (DASC)*, IEEE, New York, 2018.

[16] Cuong Chi, G., Bole, B., Hogge, E., Vazquez, S., Daigle, M., Celaya, J., Weber, A., and Goebel, K., "Battery Charge Depletion Prediction on an Electric Aircraft," *Proceedings of the Annual Conference of the Prognostics and Health Management Society*, Vol. 4, 2013, pp. 1–11.

[17] Bole, B., Daigle, M., and Gorospe, G., "Online Prediction of Battery Discharge and Estimation of Parasitic Loads for an Electric Aircraft," *Proceedings of the European Conference on the Prognostics and Health Management Society*, Vol. 5, 2014, p. 5S2P.

[18] Alnaqeb, A., Li, Y., Lui, Y., Pradeep, P., Wallin, J., Hu, C., Hu, S., and Wei, P., "Online Prediction of Battery Discharge and Flight Mission Assessment for Electrical Rotorcraft," *Proceedings of AIAA Aerospace Sciences Meeting*, AIAA Paper 2018-2005, 2018.

[19] Plett, G., *Equivalent-Circuit Methods, Battery Management Systems*, Vol. II, Artech House, Norwood, MA, 2016, pp. 69–80, Chap. 3.

[20] Goodrich, K., and Barmore, B., "Exploratory Analysis of the Airspace Throughput and Sensitivities of an Urban Air Mobility System," *Proceedings of Aviation Technology, Integration, and Operations Conference*, AIAA Paper 2018-3364, 2018.

[21] Pradeep, P., and Wei, P., "Energy Efficient Arrival with RTA Constraint for Urban eVTOL Operations," *Proceedings of AIAA Aerospace Sciences Meeting*, AIAA Paper 2018-2008, 2018, pp. 1–13.

[22] Erzberger, H., and Itoh, E., "Design Principles and Algorithms for Air Traffic Arrival Scheduling," NASA TP-2014-218302, NASA Ames Research Center, CA, 2014.

[23] "EHANG184 Autonomous Aerial Vehicle Specs," EHANG184, 2018, http://www.ehang.com/ehang184/specs/ [retrieved March 2018].

[24] Johnson, W., *Rotorcraft Aeromechanics*, Cambridge Univ. Press, Cambridge, 2013, pp. 39–81, Chap. 3.

[25] Patterson, M., and Rao, A., "GPOPS-II: A MATLAB Software for Solving Multiple-Phase Optimal Control Problems Using hp-Adaptive Gaussian Quadrature Collocation Methods and Sparse Nonlinear Programming," *ACM Transactions on Mathematical Software (TOMS)*, Vol. 41, No. 1, 2014, pp. 1–37.

[26] Samà, M., D'Ariano, A., and Pacciarelli, D., "Optimal Aircraft Traffic Flow Management at a Terminal Control Area During Disturbances," *Procedia—Social and Behavioral Sciences*, Vol. 54, No. 1, 2014, pp. 460–469.

[27] Rodriguez-Diaz, A., Adenso-Diaz, B., and Gonzalez-Torre, P., "Minimizing Deviation from Scheduled Times in a Single Mixed Operation Runway," *Computer Operations Research*, Vol. 78, Feb. 2017, pp. 193–202. https://doi.org/10.1016/j.cor.2016.09.014

M. J. Kochenderfer
Associate Editor